Lab on a Chip

Dynamic Article Links

Cite this: *Lab Chip*, 2011, **11**, 2424

www.rsc.org/loc

PAPER

A miniature capillary breakup extensional rheometer by electrostatically assisted generation of liquid filaments†

Wyatt C. Nelson,* H. Pirouz Kavehpour and Chang-Jin "CJ" Kim

Received 13th December 2010, Accepted 11th May 2011
DOI: 10.1039/c0lc00691b

A micromachined chip capable of generating liquid microfilaments has been developed for a miniature version of the Capillary Breakup Extensional Rheometer (CaBER®). The proposed system is exceptionally simple and compact because liquid samples are actuated by voltages administered on-chip, which therefore requires only electrical connections (rather than a linear motor, an integral part of the CaBER®). Since chip features are photolithographically defined, the miniature rheometer can handle sub-microlitre samples. Following the CaBER®, we show that a commercial LED micrometer effectively measures diameters of filaments generated by the electrowetting-on-dielectric (EWOD) forces. Since negligible electric fields are sustained within the liquid far away from the measurement region, the applied EWOD voltage does not influence tested material properties. Through breakup experiments using a wide range of Newtonian and complex fluids (*e.g.*, glycerol, xanthan gum, dilute polystyrene, and dilute solutions of various molecular weight polyethylene oxide) we demonstrate a versatile testing platform for scarce and precious samples such as biochemical fluids and novel materials. Measured Newtonian and complex dynamics agree well with published theories and experiments.

Introduction

There exists a wide range of commercially available extensional rheometers for measuring viscoelastic fluid properties, which are of interest in both research and industrial settings. It is important in manufacturing, for example, to understand the breakup dynamics of a polymer jet flow. A machine developed by the Cambridge Polymer Group called the Capillary Breakup Extensional Rheometer (CaBER®) accomplishes this task by subjecting fluids to a sudden elongation and monitoring the shape under a self-selected capillary-driven filament thinning process.[1–3] In this way, the fluid feels uniaxial tension similar to that imposed during a dispensing process. A similar method called Filament Stretching Extensional Rheometry (FiSER™) goes a step further by controlling the uniaxial strain and measuring the tension force in the filament.[4] While CaBER® uses a simple testing apparatus and requires careful understanding of the physics for proper data analysis, FiSER™ uses a relatively complicated apparatus that enables straightforward data analysis. Our proposed microscale platform is akin to CaBER® because filament thinning occurs at a self-selected rate, *i.e.*, the purpose of the testing apparatus is to create a state of capillary instability, which drives the breakup process. That said, our system has a different configuration than that of CaBER® and therefore attention must be paid to the fact that each system hosts slightly different flow characteristics. This is particularly important for data analysis because, while the kinematics are dominated by extensional flow, they are not purely extensional. Accounting for differences between the breakup of ideal (cylindrical) *versus* realistic (slightly necked) filaments will be discussed.

The smallest volume tested on CaBER® was a 1 μL droplet of spider silk.[5] The system was scaled-down by replacing the typical centimetre-size sample holding plates with millimetre-size plates to accommodate lower volumes. When further scaling of the mechanism as-is becomes impractical, it is appropriate to utilize microfluidic technologies, which routinely handle micro- to femtolitres. Micro- and nanofluidic approaches also enable experiments that probe surface effects and elongational behavior under exceptionally high strains.[6] The vast majority of microfluidic rheometers are channel-based chips in which flow characteristics (*e.g.*, flow rate, pressure) are measured in order to extract fluid properties, *e.g.* Newtonian shear viscosity.[7,8] There are many examples of measuring complex fluid properties utilizing resonant MEMS structures,[9–11] flow focusing,[12] electroosmosis,[13] flow-rate control of power-law liquids,[14] and electrorheological effects.[15] Lin *et al.*[16] reported a channel-based

Mechanical and Aerospace Engineering Department, University of California, Los Angeles (UCLA), 420 Westwood Plaza, Engineering IV Bldg., Room 37-129, Los Angeles, CA 90095, USA. E-mail: wyattnelson@ucla.edu

† Electronic supplementary information (ESI) available: Video S1: high speed video of GLY 50: capture rate: 30 000 fps; playback: 5 fps, Video S2: high speed video of PEO 9: capture rate: 30 000 fps; playback: 80 fps, Fig. S1: optical micrographs of etched defect patterns on chip arms, Fig. S2: minimum radii time histories of GLY 99 tested at voltages from 0 to 200 V. See DOI: 10.1039/c0lc00691b

device that uses electrowetting-on-dielectric (EWOD) as the driving mechanism instead of external pressure or electrokinetic forces. Srivastava *et al.*[17–19] reported an elegant capillary-driven, self-calibrating microchannel-based device for various fluids including blood.[20] Because of the minimal sample usage, biochemical fluids are commonly tested in microfluidic devices, *e.g.* characterizing the effects of thermal and chemical protein denaturation in blood.[20] Because liquid flow is laminar, numerical models can be paired with experiments using special channel geometries (*e.g.*, nozzles and diffusers[21]) to successfully measure complex elongational fluid properties.

Microfluidic extensional rheometry is usually accomplished by optical measurement of pinch-off in two-phase sheath flows.[22–24] In this scheme, the sample fluid is stretched by a surrounding flowing immiscible medium until capillary instabilities cause breakup, or droplet pinch-off. The minimum radius of the necking region, *i.e.*, liquid filament, is measured by optical microscopy. While the dynamics are similar, our proposed technique is simpler because the location of the minimum radius is fixed and there is no sheath flow. Like CaBER®, the EWOD-enabled platform generates liquid filaments that can be measured by a fixed optical micrometer. The potential for EWOD actuation in rheometry was demonstrated by Banpurkar *et al.*[25,26] using a sessile droplet and relating liquid properties (*e.g.* surface tension,[25] elastic modulus[26]) to the voltage-dependent measured contact angle.

In using EWOD for materials characterization, it is necessary to ensure that the applied electric fields do not affect the fluid properties of interest. Refer to the works of Mugele,[27,28] Jones[29] and Lee *et al.*[30] for descriptions of the electrical fields in EWOD, as they vary with material properties and applied frequency. These issues, however, are not a concern for our device because of the following two reasons. First, samples requiring EWOD actuation on our hydrophobic-coated device are aqueous solutions, which are conductive enough that most of the applied voltage is dropped across the solid dielectric layer (*e.g.*, over 99% for most cases) rather than within the sample. Second, the location of the measurement is far from that of EWOD actuation. The center of suspending filament is at least 100 μm away from the actuation surface, while the fringing field of the EWOD actuation reaches the order of the dielectric thickness, which is only 1 μm. Note the insulating fluids (*e.g.* styrene oil) tested here wetted the hydrophobic surface and therefore did not use EWOD actuation.

There are several potential advantages of miniaturizing the capillary breakup extensional rheometer, with the most obvious being the ability to handle small volumes (microlitres or less). Further gains include insensitivity to gravity, the possibility to integrate electronic circuits and sensors onto the testing platform through microfabrication, and the ability to develop portable (*e.g.*, handheld) systems. The apparatus reported here was designed to work with a commercial LED optical micrometer for measuring filament radii, in the same way as CaBER®. Owing to their millimetre scale dimensions, however, future systems can be coupled with sub-millimeter optical detectors.

Micromachined testing apparatus

CaBER® generates liquid filaments by separating two plates that are connected by a liquid bridge, which is the rheological sample. While commercial linear actuators are easily built into this benchtop system, it would be complicated to micromachine them for a millimetre-scale system. Rather than trying to miniaturize existing actuators, our strategy is therefore to use the surface tension of the sample, taking advantage of the favorable scaling of surface forces in the microscale. The proposed device has no moving parts and uses controlled surface properties and EWOD actuation. Depending on their electrical properties, rheological samples are pulled by EWOD forces, which are localized at liquid–solid contact lines far from the filament.[28,31,32] In this scheme, a step force is applied in order to stretch the droplet such that it is unstable, similar to the way in which CaBER® uses linear actuators to impose a step strain extending the liquid bridge to length beyond a plateau wavelength.[1] Additionally, the shape of our sample holding platform is specifically designed to facilitate the necking process and ensure that the point of measurement (*i.e.*, location of the filament minimum radius) is fixed in space.

The micromachined testing apparatus is depicted in Fig. 1. The chip consists of two parallel plates connected by a double-sided adhesive spacer (thickness = 0.5 mm). Each plate is formed by deep reactive ion etching of a standard 4″ silicon wafer (thickness = 0.5 mm). Fig. 1a is a three-dimensional sketch showing the anatomy of the chip and how it fits into a clip that provides an electrical pathway to each plate. Fig. 1b has cross-sections of a loaded chip showing that when both plates are grounded at 0 V, there is no EWOD force, and when one of the plates is biased at a DC voltage, there is an EWOD force that causes the liquid to spread onto the plate. More specifically, the electrical field at the contact line above the dielectric (silicon nitride coated by plasma-enhanced chemical vapor deposition or PECVD) gives rise to electrostatic forces pulling the charged liquid meniscus parallel to the solid surface.

The ability to stretch a liquid bridge into an unstable conformation (thus initiating breakup) is influenced not only by electrical forces, but also by the shape of the chip arms. Notice two characteristics of the arms shown in Fig. 1: (i) the arms have patterned through-holes (labeled "surface defect patterns") and (ii) the arms are tapered. These design elements were incorporated based on the following observations. With respect to (i), loading partially wetting liquids onto the chip arms using a pipette was difficult because the liquid dewetted and escaped

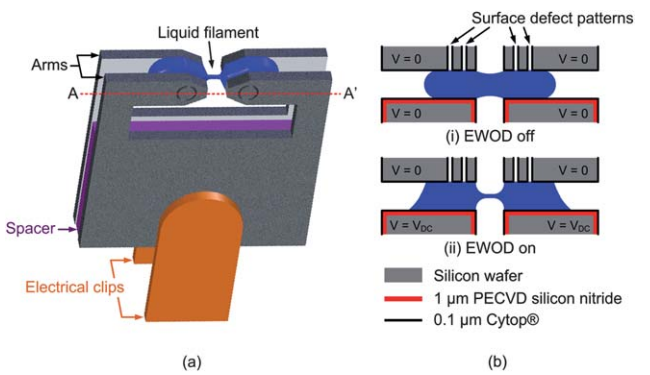

Fig. 1 (a) Three-dimensional sketch of a loaded chip and close-up of the liquid bridge. (b) Cross-sections A–A′ of (a).

from the gap between the two hydrophobic surfaces with the removal of the pipette tip. To provide resistance against dewetting, *i.e.*, to hold the sample liquid inside the gap, we have introduced artificial surface defects on the inner surface of the chip arms. Although a simple scratch on the hydrophobic coating would do the trick, we etched various defect patterns (details in the ESI†) through one plate, as shown in Fig. 1b. Since they are lithographically defined and etched simultaneously with the plates, no additional step (not even the surface scratching) needs to be added to the overall fabrication process. With respect to (ii), we found that tapered arms led to a stable and slightly necked liquid bridge after sample loading. In contrast, samples loaded onto straight arms formed a bulge in the region between the arms. Fig. 2 illustrates our observations of liquid bridges on tapered and straight arms. With straight arms, a bulge formed, and EWOD actuation produced no noticeable change of shape in the gap. This bulge formation was observed on straight arms with $w \approx g$ and $w \approx 2g$. With tapered arms, the stable bridge was slightly necked and EWOD actuation caused the necked bridge to drain and reach capillary instability. Red arrows in the figure represent the direction of fluid flow during relaxation, as indicated by the shape change. Inward-pointing arrows mean that the neck filled slightly to form a bulge, and outward-pointing arrows mean that the neck drained slightly to form a necked bridge.

A series of video frames in Fig. 3a illustrates EWOD-enabled device operation. After the sample is loaded by pipette (Fig. 3a.ii), the liquid bridge forms a stable and slightly necked liquid bridge (Fig. 3a.iii). With voltage applied to turn EWOD on (Fig. 3a.iv), the neck pinches into a filament and undergoes capillary instability-driven breakup and disappearance of the filament (Fig. 3a. v). In CaBER® the initial step strain is applied over a duration called "opening time," which is about 50 ms.[2] The analogous step in our system is the initial movement of the contact line when voltage is applied. High-speed videos of the contact line indicate that this process takes about 100 μs for 99 wt% glycerol. In CaBER® the filament cannot be measured until the plates are separated, and thus the opening time imposes a limit on operability. In our system, however, since there are no moving parts, actuation does not interfere with the optical micrometer measurement. For the EWOD-enabled rheometer experiments, opening time is a function of forced wetting dynamics, which are not well-characterized for EWOD systems,[33–35] and charging time (RC time constant of the EWOD circuit).[36]

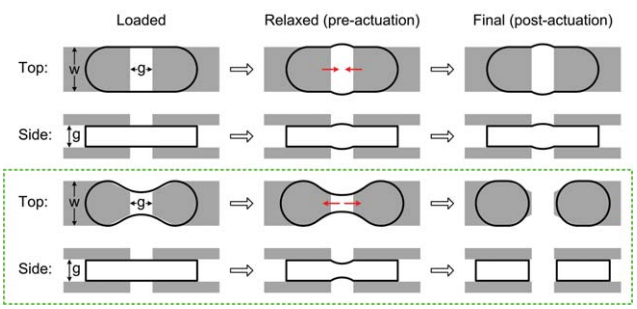

Fig. 2 Illustrations summarizing observations of partially wetting liquid samples loaded onto straight (top) and tapered (green dashed box) chip arms.

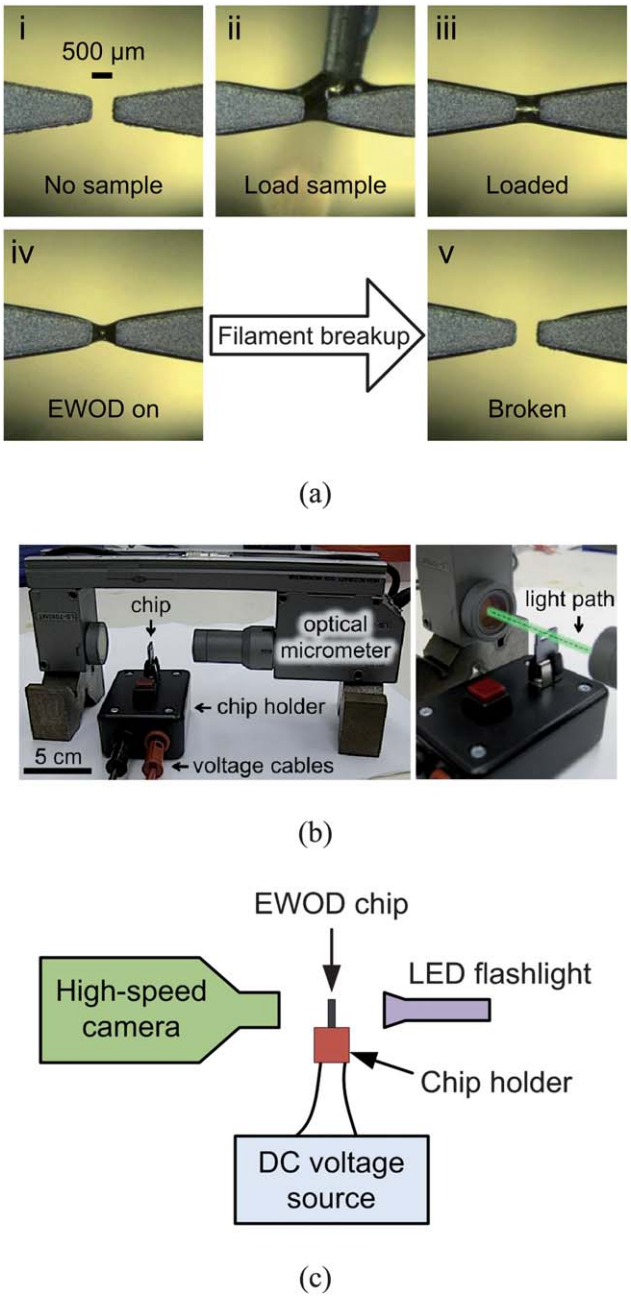

Fig. 3 (a) Close-up images of the chip arms during an EWOD-enabled breakup test: (i) clean device, (ii) pipette loading of glycerol, (iii) stable loaded sample, (iv) EWOD-assisted bridge necking, followed by capillary instability-driven filament breakup until (v) the filament is gone. Experimental setups for (b) LED optical micrometer measurements and (c) high-speed camera recording.

When testing *wetting* fluids on the reported platform, the procedure is different because the loaded sample spontaneously forms a necked liquid bridge that drains and breaks. This begs the question, "why not use a hydrophilic chip, *e.g.* glass or metal, so that EWOD is not needed?" Our reasoning for incorporating EWOD is based on controllability and ease of use. Since the electrostatic step force initiates neck drainage, the user can load the sample into a stable condition before the measurement is

taken. In contrast, if the sample spontaneously wets the chip arms, it may be difficult to test fluids that break quickly because the measurement should be started after loading and before the disappearance of the filament. For glycerol on bare silicon nitride, *i.e.*, wetting, this time window is a few milliseconds—too short for any measurement. For styrene oligomer on Cytop® (a configuration we have tested), on the other end of spectrum, this window is about 30 seconds. So, in general, wetting fluids can be tested if they are sufficiently viscous, allowing enough time between loading and initiating the measurement. This constraint does not exist with non-wetting fluids, and we therefore use a hydrophobic-coated platform to accommodate a wide range of aqueous liquids.

Experimental setup

In this study we used two experimental measurement techniques: LED optical micrometry (Keyence LS-7000 Series) to measure the diameter of the thinning film and high-speed photography (Phantom V 7.2) to confirm accuracy and reliability of the LED micrometer measurement. Fig. 3b shows a picture of the optical micrometer setup, and Fig. 3c is a schematic representation of the high-speed camera setup. High-speed video frames were extracted and analyzed by a custom MATLAB® code, which measured the minimum diameter of the liquid filament. By observing breakup using the high-speed camera, we were able to verify that LED micrometer data captured the same dynamics.

Filament breakup dynamics

Proper analysis of capillary breakup data requires an adequate understanding of the flow characteristics because they are self-selected, *i.e.*, liquid deformations are determined by intrinsic stresses. Our simple analysis to follow, which is based on that used by the developers of CaBER®,[1–3,37] is carried out under the assumption that simple uniaxial extension of the liquid filament dominates the evolution of its minimum radius. The validity of this assumption may be tested by several factors, notably including end effects: shear stresses within the fluid caused by flow over the solid surfaces that hold/pull the sample. Also, in our case, we must be assured that applied electric fields impose negligible stresses on the liquid near the measurement.

Spiegelberg *et al.*[38] provide a thorough study of end effects in a filament stretching device, showing that, especially at low total strain, shear imposed by the sample holding plates can significantly affect the filament dynamics. Importantly, the end plates move continuously during a filament stretching measurement; the end plates are fixed during capillary breakup measurements. The latter point leads to the assumption that during a CaBER® measurement the liquid volumes held by the end plates are quasi-static, low-pressure reservoirs into which liquid from the high-pressure filament drain. Similarly, the proposed electrostatically enabled chip has no moving parts. In our case, the quasi-static assumption is supported by the following scaling argument: by mass conservation the flow rates in the filament and the reservoir are equal, *i.e.*, $v_f A_f = v_r A_r$, where v is the mean velocity and A is the cross-sectional area. The characteristic dimensions of our measured filaments and end plates are such that $v_f/v_r \approx (10^{-3}/10^{-4})^2 = 10^2$, implying that the extensional flow in the filament is dominant over flow in the reservoir.

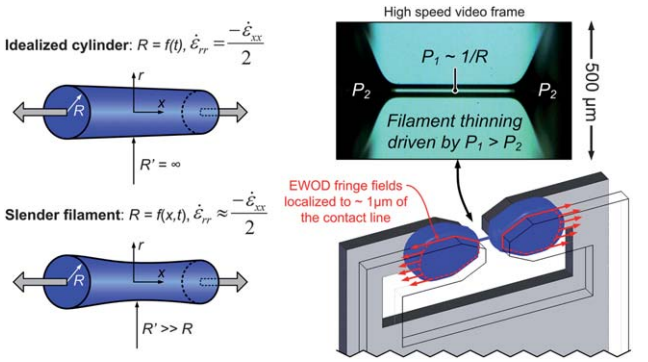

Fig. 4 Left: illustrations of idealized and realistic filament shape. Right: a high-speed video frame showing a measured PEO 9 filament, and a 3-dimensional schematic of the rheometer chip with red lines indicating the location of EWOD fringe fields.

Simple uniaxial extension applies to the ideal case of a perfect liquid cylinder.[39] Fig. 4 has a pictorial comparison of an idealized cylindrical filament *versus* a more realistic slender filament. The key difference is that the latter filament has an associated axial radius of curvature R' in addition to R, the dominant radius of curvature. In the ideal case, R is only a function of time, and in the realistic case R is a function of the axial direction x as well as time. In our experiments, we observed that in the beginning of breakup, R' is comparable to the distance between the sample holding arms. After R has dropped below a certain critical value (apparently depending on the viscosity and elasticity of the fluid), the axial curvature ($1/R'$) becomes very small compared to the radial curvature ($1/R$), and based on the self-similarity solutions of filament thinning[40–42] as well as the results of Rodd *et al.*[2] we expect that R' is then independent of the device dimensions. Further characterization will be necessary to determine the variation of the critical R value (or Hencky strain $= -2\ln(R/R_0)$) with device dimensions and fluid properties.

Fig. 4 also includes 3-dimensional schematic showing the locations of EWOD fringing fields that result in liquid motion. As stated above, the fringe fields are expected to extend over a length scale comparable to the dielectric thickness (~1 μm), which falls far short of reaching the filament. With the application of DC voltage, there is an associated RC time constant that provides an estimate of how long it takes for the applied field to be shielded from the liquid bulk. This time constant, which has been derived by several authors as a "cutoff frequency" below which EWOD forces localized to the dielectric layer,[36,43,44] has the following simplified form: $\tau \approx (c_l + c_d)/g_l$, where $c = \varepsilon_0\varepsilon_r/t$ are specific capacitances, ε_0 is the permittivity of free space, ε_r is the relative permittivity, t is the layer thickness, and $g_l = \sigma_l/t_l$ is the specific conductance of the liquid. For our case, the worst-case scenario is approximated as follows for the actuation of glycerol (with room temperature conductivity $\sigma_l \approx 6 \times 10^{-6}$ S m^{-1} and dielectric constant $\varepsilon_l \approx 40$): $\tau \approx 3$ ms, where $\varepsilon_d = 4$, $t_d = 1$ μm, and $t_l = 500$ μm. Even with this low conductivity liquid, the bulk is expected to be shielded from electric fields long before filament breakup ensues, >100 ms after the application of voltage.

To investigate whether or not measurements are sensitive to EWOD fields, we tested glycerol using a range of voltages (0 to 200 V), and measured minimum radii, R_{min} (details in the ESI†).

After slight variations early in the breakup process, the R_{min} data collapse onto a single line, indicating that the thinning dynamics were insensitive to applied voltage. Since voltages below 80 V did not provide enough force to initiate filament generation, a different method was used in order to test the 0 V case: a hydrophilic wire was placed within each chip arm upon sample loading, causing the liquid bridge between the arms to drain and breakup.

In discussing the flow regimes observed on the device, we will consider three filament breakup timescales, the longest of which corresponding to the dominating physical mechanism of the process. These timescales are:

$$\text{Inertial} \quad t_i \propto \sqrt{\rho L^3/\gamma} \quad \rho : \text{density}; L : \text{characteristic length};$$

$$\gamma : \text{surface tension}$$

$$\text{Viscous} \quad t_v \propto \eta L/\gamma \quad \eta : \text{viscosity}$$

$$\text{Elastic} \quad t_e = f(\lambda, \gamma, \eta, L) \quad \lambda : \text{stress relaxation time}$$

In capillary instability-driven breakup, the dynamics are self-selected, *i.e.*, the dominant force opposing surface tension (which drives thinning) depends on the fluid properties and filament dimensions. The above relationships for inertial and viscous timescales are apparent from simple force scaling analyses, balancing surface tension ($F \propto \gamma A/L$; A = area) with inertia ($F \propto \rho A(\mathrm{d}L/\mathrm{d}t)$) or viscosity ($F \propto \eta A L^{-1}(\mathrm{d}L/\mathrm{d}t)$). We have left the scaling relationship for elastic breakup in general terms because there are several stages, each with a distinct functional relationship for strain rate. For example, at early stages of breakup, the strain rate is limited by solvent viscosity. At intermediate stages, the strain rate is limited by the molecular stress relaxation time and is independent of surface tension and solvent viscosity. In this regime the filament radius decays exponentially and thus does not break.[40] At late stages, a finite extensibility limit is reached, and the filament decays linearly until it vanishes. The stages of elastic filament breakup are described in detail by Entov and Hinch.[40]

Newtonian fluids do not exhibit elasticity, and visco-capillary breakup is observed when $t_v > t_i$. To predict actual values of t_v, McKinley and Tripathi proposed the following linear relationship and found it to be consistent with experiments performed using CaBER® when $X = 0.7127$, the solution of Papageorgiou for a viscous liquid thread.[1,41]

$$R_{min}(t) = R_1 - \frac{(2X-1)}{6}\frac{\gamma}{\eta_S}t \tag{1}$$

This equation is arrived at by integrating the balance of viscous and surface tension stresses: $\eta_E\,\dot{\varepsilon} = \gamma(2X-1)/R_{min}$ with the strain rate $\dot{\varepsilon} = -2\mathrm{d}R_{min}/R_{min}\mathrm{d}t$, a dimensionless parameter X accounting for axial curvature, and the extensional viscosity $\eta_E = 3\eta_S$. The latter relationship is a restatement of the known result $Tr = 3$, where the Trouton ratio (Tr) is defined as the ratio of extensional (η_E) to zero-shear viscosity (η_0).[45,46] A full derivation of eqn (1) is provided by McKinley and Tripathi; note that ours is highly simplified for the sake of brevity. Refer to Fig. 4 for a clarification on the relationships between axial strain and radial strain for an ideal cylinder and a slender filament. In the latter case, the relationship is not exact, which is the reason why $X = 1$ (the expected solution when axial curvature is neglected) does not match experimental results. Other values of X have been proposed for various flow regimes, which are discussed by McKinley and Tripathi.[1] Upon experimental verification, the solution with $X = 0.7127$ was deemed most appropriate for viscous fluids in CaBER®.

Complex fluids exhibiting elasticity demand a more complex description of filament thinning dynamics. As described above, filaments undergo several stages of thinning, each dominated by a different mechanism, *e.g.*, solvent viscosity, polymer chain relaxation, fully extended and aligned polymer chains. As explained by Entov and Hinch,[40] there is likely to be a multitude of relaxation times characterizing the polymer extension stage. The minimum radius can therefore be expected to follow the form:[3]

$$\frac{R_{min}(t)}{R_1} = \left(\sum_i \frac{G_i R_1}{\gamma}\exp\left(-t/\lambda_i\right)\right)^{1/3}. \tag{2}$$

This expression corresponds to the elasto-capillary stage of thinning, when solvent viscosity is negligible and finite extensibility limits have not been reached. Further, eqn (2) is limited to the cases of dilute solutions of non-interacting finitely extensible nonlinear elastic (FENE) dumbbells having elastic moduli G_i and relaxation times λ_i. Anna and McKinley[3] describe that, for solutions well-described by the Rouse-Zimm model, eqn (2) simplifies to the form: $R_{min}(t) = R_1(\lambda_Z\gamma/2\eta_0 R_1)^{1/3}\exp\left(-t/3\lambda_Z\right)$,[47] where the Zimm (longest) relaxation time λ_Z can be estimated by regressing capillary breakup data to this expression.

With respect to practical applications involving extensional flows, it is instructive to track the apparent extensional viscosity as it varies with strain. Balancing viscous, elastic, and surface tension contributions, one arrives at an apparent extensional viscosity $\eta_{APP} = -\gamma/2\mathrm{d}R_{min}/\mathrm{d}t$.[3] To calculate values of η_{APP} from measurements of R_{min}, we follow a previously reported method[48] by first regressing the data to the following equation before taking the derivative:

$$R_{min}(t) = A\exp\left(\frac{-t}{B}\right) + Ct + D. \tag{3}$$

A, B, C, and D are fitting parameters related to liquid properties including surface tension and elasticity. The above equation has exponential and linear terms intended to account for the different stages of visco-elasto-capillary breakup described above. In other words, the exponential term attempts to describe the polymer extension stage, and the linear term corresponds to the stage in which polymer chains are fully extended.

Results and discussion

As introduced in a preliminary report,[49] we have observed visco-capillary and visco-elasto-capillary breakup on a microextensional filament rheometer enabled by EWOD. These included demonstrations using styrene oligomer, polystyrene Boger fluid (PS 0.025 wt%), and aqueous shear-thinning xanthan gum (1 wt %), and glycerol solutions. We have also verified the use of an LED optical micrometer as an accurate measurement tool with our system. Fig. 6a is a plot summarizing data from the above

four fluids representing a wide range of viscous fluids. For easy comparison, the data are plotted in non-dimensional form, R_{min}/R_1 *versus* t/t_b, where R_1 (about 60 μm for each liquid) was chosen as a filament radius below which R_{min} was observed to follow a clear trend, *e.g.*, linear or exponential. There is an initial stage of filament thinning preceding the stage in which R_{min} follows our expected trend, *i.e.*, linear visco-capillary breakup. The breakup time t_b is the time it takes for R_{min} to drop from R_1 to below the minimum measurement of $R_{min} \approx 5$ μm.

An important feature of Fig. 6a is that optical micrometer data match high speed camera measurements, verifying that the former method is accurate. This is encouraging because, given the millimetre dimensions of our platform, we see an opportunity to use a similarly sized, possibly microfabricated, LED-based measurement system. For this study, we used the off-the-shelf Keyence system because it is similar to that which is part of CaBER®, but (as evident in Fig. 3b) it is unnecessarily large. It should also be noted that the minimum measurement we achieved with the optical micrometer was about $R_{min} \approx 20$ μm, but others have reported that proper tuning can lead to reliable measurements down to 5 μm.[2]

The shear-thinning xanthan gum solution exhibits an approximately linear decay, resembling a Newtonian liquid. Xanthan gum is known to be elastic, but since the molecules are rigid, variations of extensional viscosity with ε are attributable to alignment of polymer chains and not stretching.[50] This has two main consequences with respect to our breakup experiments: (i) compared to relatively compliant molecules, *e.g.*, PEO, xanthan gum is weakly elastic, and (ii) elastic effects are only present in the initial stages of extension, after which the molecules are aligned and the solution exhibits an extension viscosity is not a function of ε.[51]

Note that EWOD actuation was not used for the measurement styrene oligomer and PS 0.025 wt%. Instead, once loaded onto the chip, their wetting to the inner surfaces of the chip was strong enough to stretch the droplet spontaneously. In these cases, there was sufficient time (~30 s) between sample loading and capillary breakup to initiate the measurement. In contrast, the breakup of xanthan gum and glycerol solutions was triggered by EWOD; they were brought to instability by applying 100 V_{DC} for less than one up to several seconds to initiate filament thinning.

To explore a wider range of operability we tested solutions of polyethylene oxide (PEO), demonstrating that the EWOD step force can be used to trigger elasto-capillary breakup of low-viscosity liquids. Further, a range of PEO molecular weights were tested in order to verify that the reported system properly measures the expected increase in stress relaxation time with molecular weight.[24,47] Table 1 lists properties and dimensionless quantities of all tested fluids, including PEO dissolved in 1 : 1 mixtures of glycerol and deionized water. The dimensionless parameters Ohnesorge number and Deborah number are defined following Rodd *et al.*[2] for fluid threads as: $Oh = \eta_S/\sqrt{\rho R_0 \gamma} = t_v/t_i$ and $De = \lambda_Z \Big/ \sqrt{\rho R_0^3/\gamma} = \lambda_Z/t_i$, in which λ_Z are values extracted from our experiments by fitting an exponential decay to the minimum filament radius data. Quantities in Table 1 were computed using published viscosities[52] ($\eta_{GLY\ 99} = 700$ Pa·s, $\eta_{GLY\ 50} = 5$ mPa·s), $R_0 = 100$ μm, $\rho = 1000$ kg m^{-3}, and $\gamma = 65$ mN m^{-1}. Rodd *et al.*[2] define a "low-viscosity fluid" as that for which $Oh < 0.14$. Values of c^* were calculated using the Mark–Houwink relationship for intrinsic viscosity with Graessley's expression for c^*, as described in ref. 2. The *De* is an intrinsic quantity expressing the relative influence of elasticity and inertia in breakup dynamics.

Fig. 5a compares high-speed video frames from the breakup of GLY 99 and GLY 50. GLY 99 undergoes a visco-capillary process, *i.e.* $t_v > t_i$, and the opposite is true for the latter case. The frame numbers (captured at 30 kfps) indicate that the viscous breakup takes much longer as the liquid forms a slender filament before it vanishes. The thinning of the GLY 50 liquid bridge,

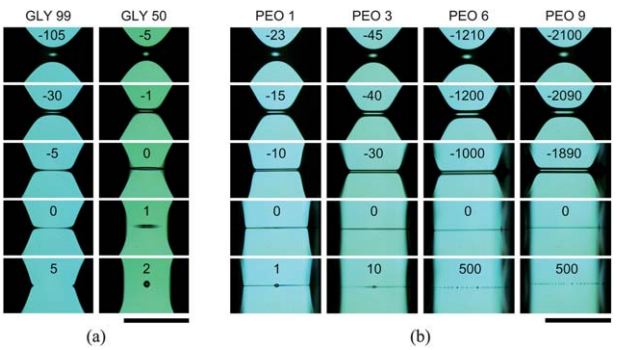

Fig. 5 (a) High-speed video frames of viscous (GLY 99) and inertial (GLY 50) breakup of aqueous glycerol solutions. Frame zero is assigned to the frame before the filament disappears. (b) High-speed video frames of elastic breakup of aqueous glycerol + PEO solutions. Frame zero is assigned to the frame before beads-on-a-string form along the filament. For both (a) and (b), frames were captured at a rate of 30 000 fps. The scale bars are 0.5 mm. See videos of GLY 50 and PEO 9 in the ESI†.

Table 1 Testing fluid properties

Name	M_w/g mol^{-1}	Polymer (% w/w)	Glycerol (% w/w)	c/c^{*a}	*Oh*	$\lambda_Z{}^b$/s	De^b
GLY 99	—	—	99	—	9	—	—
GLY 50	—	—	50	—	0.06	—	—
PEO 1	1×10^5	0.05	50	0.08	—	$1.4 \pm 0.3 \times 10^{-4}$	1
PEO 3	3×10^5	0.05	50	0.17	—	$4.0 \pm 1.5 \times 10^{-4}$	3
PEO 6	6×10^5	0.05	50	0.27	—	$5.5 \pm 1.2 \times 10^{-3}$	43
PEO 9	9×10^5	0.05	50	0.35	—	$1.0 \pm 0.1 \times 10^{-2}$	80
Oligomer	—	—	—	—	1050	—	—
PS 0.025	2×10^6	0.025	—	0.30	—	5.7 ± 1.0	3×10^4

[a] c^*: coil overlap concentration; *Oh*: Ohnesorge number; *De*: Deborah number. [b] λ_Z and *De* calculated using measured values.

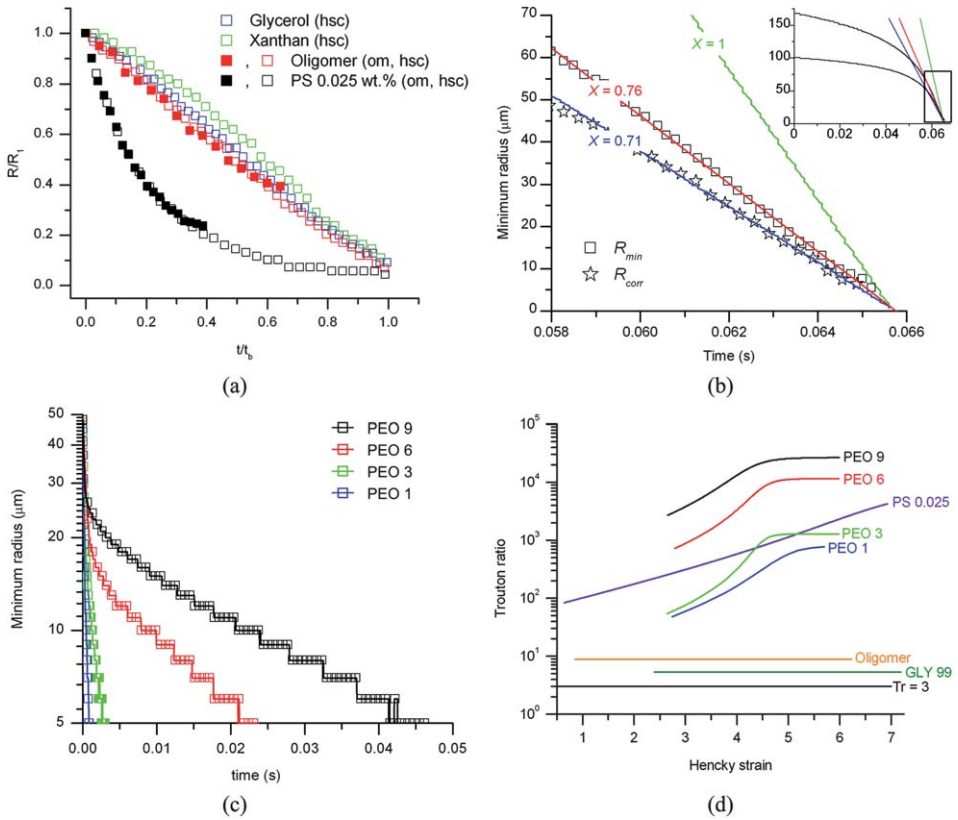

Fig. 6 (a) Dimensionless plot summarizing filament breakup data for various fluids of minimum radii measured by a high-speed camera (hsc, hollow symbols) and optical micrometer (om, filled symbols). (b) Minimum filament radii of 99 : 1 glycerol–water solution (GLY 99). The large plot is a blow-up of the region outlined by a red rectangle in the inset. Lines are solutions of eqn (1) for $X = 0.71$, 0.76, and 1. (c) Minimum filament radii for various molecular weight PEO solutions. (d) Predicted apparent extensional viscosities calculated *via* differentiation of eqn (3) and plotted in terms of Trouton ratio *versus* Hencky strain.

however, is not slowed much by viscosity and therefore breaks up rapidly before becoming a filament. Minimum filament radii extracted from the GLY 99 breakup videos are shown in Fig. 6b. The large plot is a blow-up of the region outlined in red in the inset. This portion of the graph corresponds to the thinning of a long slender filament, which is expected to decay linearly. Directly fitting eqn (1) to the data yields a value $X = 0.76$, which is slightly larger than Papageorgiou's self-similarity solution ($X = 0.7127$)[41] and smaller than the solution $X = 1$ predicted for a capillary–viscous force balance on an ideal liquid cylinder.[40] The discrepancy between our experimental result and that of McKinley and Tripathi,[1] who verified the use of $X = 0.7127$, can be attributed to the fact that each system has a different configuration. In our case, to extract quantitatively accurate viscosities, we expect that it will be necessary to account for the fact that the liquid held between the chip arms is not at atmospheric pressure. For example, in the case of glycerol we expect that the EWOD forces applied at the ends of the liquid cause a suction (negative meniscus curvature) having a characteristic radius $R_{end} \approx 250$ μm, half the distance between the chip plates. A simple way to incorporate this effect is by a corrected minimum radius: $R_{corr} \equiv R_{min}R_{end}/(R_{min} + R_{end})$, which is analogous to an equivalent capacitance of two capacitors in series. Fig. 6b includes R_{corr} data, which yield $X = 0.71$ when regressed to eqn (1). While this agreement with Papageorgiou's solution may be fortuitous, the use of R_{corr} demonstrates the important point that the expression used to extract fluid properties from measurements must be appropriate for the device configuration and cannot necessarily be borrowed directly from another similar platform CaBER®.

To observe the effect of molecular weight on thinning dynamics, various aqueous glycerol + PEO solutions were tested on the EWOD-enabled platform. Fig. 5b shows high-speed video frames, in which a clear trend is observed: filaments of high molecular weight PEO solutions last longer than those of relatively low molecular weight solutions. Frame zero is assigned to the moment before beads-on-a-string form along the filament. Minimum filament radius data extracted from the PEO solution breakup videos are shown in Fig. 6c. Estimated Zimm relaxation times (λ_Z), based on fitting an exponential to the data, are listed in Table 1, and these values are consistent with data obtained from CaBER® experiments using similar PEO solutions.[2]

Apparent extensional viscosities are estimated by fitting R_{min} data to eqn (3) (with the square of the correlation coefficient greater than 0.99), taking its derivative, and plugging the result into the following equation: $\eta_{APP} = -\gamma/2\mathrm{d}R_{min}/\mathrm{d}t$. In Fig. 6d, the apparent extensional viscosities are plotted in terms of Trouton ratio (η_{APP}/η_0) *versus* Hencky strain (2ln (R_0/R_{min}), with $R_0 =$ 200 μm). For this calculation, R_0 is the approximate radius of the necked liquid bridge prior to EWOD actuation. For PEO

solutions, we see the expected trend that the Trouton ratio varies by orders of magnitude with the molecular weight. Also, the reader will notice that the Newtonian fluids do not fall on $Tr = 3$; this occurs because the equation for η_{APP} has $X = 1$ for simplicity. As shown for glycerol solutions, an adjusted value of X is necessary to yield quantitatively accurate shear viscosities from the capillary breakup measurement. The disagreement between Trouton ratios of glycerol and oligomer needs to be resolved. We expect this will be accomplished by inserting a correction factor that accounts for wetting properties, device dimensions, and their effects on the capillary driving pressure during breakup. This will accompany further investigations into the effects of chip arm geometries.

Conclusions

We have discussed the design and demonstration of a micromachined chip that generates liquid filaments from microlitre samples for miniaturized capillary breakup extensional rheometry. The chip uses an EWOD configuration for electrostatic actuation of non-wetting liquids. The presence of applied voltages was not expected to influence the measured fluid properties. The minimum radius data obtained from our system using optical micrometry and high-speed photography have been shown to accurately capture a range of viscous and elastic capillary breakup dynamics, and extracted fitting parameters agree well with published values.

Acknowledgements

The authors would like to thank Dr. Prosenjit Sen for his sound advice, and Jeremy Shubert for demonstrating the optical micrometer. This work was supported by an NSF Integrative Graduate Education and Research Traineeship (DGE-0654431) through the UCLA Materials Creation Training Program (MCTP) and the NSF Graduate Research Fellowship Program (DGE-0707424).

References

1 G. H. McKinley and A. Tripathi, *J. Rheol.*, 2000, **44**, 653.
2 L. E. Rodd, T. P. Scott, J. J. Cooper-White and G. H. McKinley, *Appl. Rheol.*, 2005, **15**, 12–27.
3 S. L. Anna and G. H. McKinley, *J. Rheol.*, 2001, **45**, 115–138.
4 S. L. Anna, G. H. McKinley, D. A. Nguyen, T. Sridhar, S. J. Muller, J. Huang and D. F. James, *J. Rheol.*, 2001, **45**, 83–114.
5 N. Kojić, J. Bico, C. Clasen and G. H. McKinley, *J. Exp. Biol.*, 2006, **209**, 4355–4362.
6 C. J. Pipe and G. H. McKinley, *Mech. Res. Commun.*, 2009, **36**, 110–120.
7 Y. J. Kang, S. Y. Yoon and S. Yang, in *Proc. Int. Conf. MEMS*, Hong Kong, China, 2010, pp. 71–74.
8 P. Galambos and F. Forster, in *Proc. Int. Conf. MEMS*, Heidelberg, Germany, 1998, pp. 187–191.
9 R. L. Borwick, III, P. A. Stupar and J. F. DeNatale, in *Proc. Conf. Solid-State Sensors, Actuators, and Microsystems Workshop*, Hilton Head, South Carolina, USA, 2006, pp. 340–343.
10 O. Brand, J. M. English, S. A. Bidstrup and M. G. Allen, in *Proc. Int. Conf. Solid-State Sensors and Actuators*, Chicago, Illinois, USA, 1997, pp. 121–124.
11 D. Sparks, R. Smith, V. Cruz, N. Tran, A. Chimbayo, D. Riley and N. Najafi, *Sens. Actuators, A*, 2009, **149**, 38–41.
12 N.-T. Nguyen, Y.-F. Yap and A. Sumargo, *Meas. Sci. Technol.*, 2008, **19**, 085405.
13 T. J. Craven, J. M. Rees and W. B. Zimmerman, *Microfluid. Nanofluid.*, 2010, **9**, 559–571.
14 H. C. H. Bandalusena, W. B. Zimmerman and J. M. Rees, *J. Non-Newtonian Fluid Mech.*, 2010, **165**, 1302–1308.
15 J. Chevalier and F. Ayela, *Rev. Sci. Instrum.*, 2008, **79**, 076102.
16 Y.-Y. Lin, C.-W. Lin, L.-J. Yang and A.-B. Wang, *Electrochim. Acta*, 2007, **52**, 2876–2883.
17 N. Srivastava, R. D. Davenport and M. A. Burns, *Anal. Chem.*, 2005, **77**, 383–392.
18 N. Srivastava and M. A. Burns, *Anal. Chem.*, 2006, **78**, 1690–1696.
19 N. Srivastava and M. A. Burns, *Lab Chip*, 2006, **6**, 744–751.
20 S. Choi and J.-K. Park, *Small*, 2010, **6**, 1306–1310.
21 M. S. N. Oliveira, M. A. Alves, F. T. Pinho and G. H. McKinley, *Exp. Fluids*, 2007, **43**, 437–451.
22 B. Steinhaus, A. Q. Shen and R. Sureshkumar, *Phys. Fluids*, 2007, **19**, 073103.
23 P. E. Arratia, J. P. Gollub and D. J. Durian, *Phys. Rev. E: Stat., Nonlinear, Soft Matter Phys.*, 2008, **77**, 036309.
24 P. E. Arratia, L.-A. Cramer, J. P. Gollub and D. J. Durian, *New J. Phys.*, 2009, **11**, 115006.
25 A. G. Banpurkar, K. P. Nichols and F. Mugele, *Langmuir*, 2008, **24**, 10549–10551.
26 A. G. Banpurkar, M. H. G. Duits, D. van den Ende and F. Mugele, *Langmuir*, 2009, **25**, 1245–1252.
27 F. Mugele and J. Buehrle, *J. Phys.: Condens. Matter*, 2007, **19**, 375112.
28 F. Mugele and J.-C. Baret, *J. Phys.: Condens. Matter*, 2005, **17**, 705–774.
29 T. B. Jones, *Mech. Res. Commun.*, 2009, **36**, 2–9.
30 H. Lee, K.-S. Yun, S. H. Ko and K. H. Kang, *Biomicrofluidics*, 2009, **3**, 044113.
31 K. H. Kang, *Langmuir*, 2002, **18**, 10318–10322.
32 T. B. Jones, *J. Micromech. Microeng.*, 2005, **15**, 1184–1187.
33 T. D. Blake, A. Clarke and E. H. Stattersfield, *Langmuir*, 2000, **16**, 2928–2935.
34 R. Bavière, J. Boutet and Y. Fouillet, *Microfluid. Nanofluid.*, 2008, **4**, 287–294.
35 P. Sen and C.-J. Kim, *Langmuir*, 2009, **25**, 4302–4305.
36 T. B. Jones, J. D. Fowler, Y. S. Chang and C.-J. Kim, *Langmuir*, 2003, **19**, 7646–7651.
37 M. Cromer, L. P. Cook and G. H. McKinley, *Chem. Eng. Sci.*, 2009, **64**, 4588–4596.
38 S. H. Spiegelberg, D. C. Ables and G. H. McKinley, *J. Non-Newtonian Fluid Mech.*, 1996, **64**, 229–267.
39 C. W. Macosko, *Rheology: Principles, Measurements, and Applications*, Wiley-VCH, New York, 1994.
40 V. M. Entov and E. J. Hinch, *J. Non-Newtonian Fluid Mech.*, 1997, **72**, 31–53.
41 D. T. Papageorgiou, *Phys. Fluids*, 1995, **7**, 1529–1544.
42 J. Eggers, *Rev. Mod. Phys.*, 1997, **69**, 865–929.
43 T. B. Jones and K.-L. Wang, *Langmuir*, 2004, **20**, 2813–2818.
44 D. Chatterjee, H. Shepherd and R. L. Garrell, *Lab Chip*, 2009, **9**, 1219–1229.
45 F. T. Trouton, *Proc. R. Soc. London, Ser. A*, 1906, **77**, 426–440.
46 C. J. S. Petrie, *J. Non-Newtonian Fluid Mech.*, 2006, **137**, 15–23.
47 C. Clasen, M. Verani, J. P. Plog, G. H. McKinley and W.-M. Kulicke, in *Proc. Int. Conf. Rheol.*, 2004.
48 A. Bhardwaj, E. Miller and J. P. Rothstein, *J. Rheol.*, 2007, **51**, 693–719.
49 W. Nelson, P. Kavehpour and C.-J. Kim, in *Proc. Int. Conf. MEMS*, Hong Kong, China, 2010, pp. 75–78.
50 L. B. Smolka and A. Belmonte, *J. Non-Newtonian Fluid Mech.*, 2006, **137**, 103–109.
51 M. A. Zirnsak, D. V. Boger and V. Tirtaatmadja, *J. Rheol.*, 1999, **43**, 627–649.
52 http://www.dow.com/glycerine/resources/table18.htm.